Available online at www.sciencedirect.com
SCIENCE DIRECT®
Journal of Nuclear Materials 325 (2004) 1–12
journal of nuclear materials
www.elsevier.com/locate/jnucmat

Helium diffusion in uranium and plutonium oxides

C. Ronchi *, J.P. Hiernaut

European Commission, Joint Research Centre, Institute for Transuranium Elements, Postfach 2340, 76125 Karlsruhe, Germany

Received 17 June 2003; accepted 13 October 2003

Abstract

Samples of UO_2, $(U,Pu)O_2$ and PuO_2 containing up to several 100 at. ppm helium were submitted to thermal annealing in a Knudsen-cell provided with a mass spectrometer. Gas release was measured on line with a great accuracy. In the examined materials helium was created by α-decay of plutonium or laboratory infused at high temperature and high pressure. The selected samples exhibited different types of lattice damage, including reactor burn-up and high α-radiation doses. Analysis of helium release as a function of temperature enabled the elementary diffusion processes to be investigated and the atomic diffusion coefficient to be deduced for a defined state of helium-in-solid. The helium diffusion coefficient has the expression:

$$D = 8 \times 10^{-7} \exp(-46\ \text{kcal mol}^{-1}/RT)\ \text{m}^2\,\text{s}^{-1},$$

however, the enthalpy of diffusion increases to 70 kcal mol^{-1} in high burn-up fuel where helium is apparently stabilised in uranium/oxygen vacancy clusters.

1. Introduction

In nuclear reactor fuel an important amount of helium is produced by α-decay of initial fissile atoms and heavier nuclides formed by neutron capture. This effect is of some relevance in fast breeder reactors where much larger amounts of plutonium and minor actinides are present than in thermal reactors. However, since fast reactor fuel is mostly operated under high fission-gas release regimes, the presence of additional helium has practically no effect on the fuel behaviour. For this reason, only few experiments have been carried out so far on diffusion of helium in uranium and plutonium mixed oxides.

This issue is, however, receiving increasing attention in the context of current actinides transmutation programmes. In these tests, minor actinides are dispersed in appropriate targets with concentrations up to 20 at.% and irradiated in nuclear reactors. Most minor actinides undergo fission only with a lesser yield, whilst the majority of them are transformed in short-lived nuclides that eventually decay into more stable radionuclides along α-emission chains. The yield of helium created by actinide transmutation is, therefore, at least four times larger than that of xenon and krypton created by fission.

The effect of large concentrations of helium in actinide dioxides is still matter of investigation. A priori conjectures that small helium atoms can be readily accommodated in the relative large octahedral interstitial sites of the host fluorite lattice of these oxides are in practice contradicted by dramatic effects observed after accumulation of helium at low temperature in fuels containing large concentrations of α-emitters. For instance, PuO_2 pellets fabricated in our laboratory in the 1960s after four decades storage in an inert atmosphere (N_2), though apparently geometrically intact, do completely disaggregate under normal handling (Fig. 1). Though it is well known that helium produces embrittlement in metals, such a dramatic effect as shown in Fig. 1 was never observed neither in uranium dioxide pellets nor in oxide fuel samples submitted to comparable

* Corresponding author.
E-mail addresses: ronchi@itu.fzk.de (C. Ronchi). hiernaut@itu.fzk.de (J.P. Hiernaut)

0022-3115/$ - see front matter © 2003 Elsevier B.V. All rights reserved.
doi:10.1016/j.jnucmat.2003.10.006

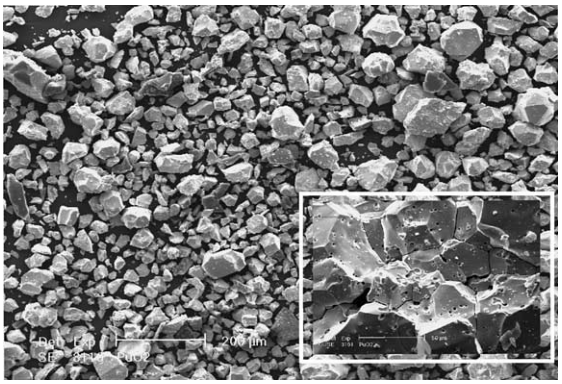

Fig. 1. SEM micrograph showing disintegration of a PuO_2 pellet after 40 years storage under nitrogen atmosphere. Helium accumulation was likely the cause of extreme embrittlement. The inset shows that all the grains are separated.

damage doses in ion implantation experiments. Actually, several questions must be answered concerning the behaviour of helium both during irradiation and also in spent fuel during long time storage. The first one regards the diffusion and precipitation/release conditions. This paper presents experimental results demonstrating that diffusion of helium in fuel is essentially different from that of fission gas, but is similarly governed by complex mechanisms which need in-depth analysis.

2. Experimental setup

Helium release measurements have been carried out in a Knudsen-cell facility where a quadrupole mass spectrometer (MS) was placed at a distance of 50 mm from the cell aperture. The cell was made of tungsten and operated under an ultra high vacuum up to temperatures of 2800 K. Though release of gas-in-solid is obviously occurring under cell effusion conditions far from thermodynamic equilibrium, the emitted gas/vapour beam is sufficiently regular to enable a quantitative mass spectrometric analysis of the intensity of the emitted vapour/gas to be carried out. Yet, whilst effusing condensable vapour molecules pass only once through the ionising electron beam of the MS, gas atoms must be trapped in order that they are not re-entering in the ion source after colliding with the containment wall. In the present setup the ion source is surrounded by a powerful liquid nitrogen trap on which most gaseous species travelling outside the collimated effusion beam are condensed. Yet, since helium is unaffected by this trap, its mass spectrometric signal is depending not only on the molecular beam intensity, but also on the average residence time of the atoms in the ion source chamber and hence on the evacuating flow through the operating turbo-molecular pumps. In spite of repeated efforts, direct calibration method for helium resulted to be rather imprecise. Calibration tests on samples containing known amounts of helium gave uncontrolled variations of the yield of the mass spectrometer of up to 20%, against 1% for condensable species. Therefore, a complex spike analysis is presently being implemented for gases, whose realisation will however require major changes in the setup. Nevertheless, though the measured *absolute* amount of gas effusing from the cell is rather imprecise, by applying a suitable temperature programme, the *total* amount of helium initially present in the sample could be released during the experiments, so that the *fractional* release curve was obtained with a sensitivity of better than 100 at. ppm of the helium inventory.

3. Samples

Three different kinds of materials were used in the reported experiments: (a) UO_2 and MOX fuel irradiated in LWR at low temperature and different burn-ups; (b) PuO_2 and $(U,Pu)O_2$ pellets sintered from mechanically blended powder and from solid solutions particles (fabricated by a sol–gel process) containing 10 at.% ^{238}Pu and stored for several years to accumulate alpha-helium; (c) uranium dioxide pellets melted by laser heating in an autoclave under 2000 bar helium. Relevant features of the samples are reported in Tables 1 and 2.

The selected materials are respectively suitable for investigating diffusion of helium in concomitance with fission gas, under alpha-damage conditions, and in a state of thermodynamically solution in solid.

The samples were in the form of small fragments of approximately 1 mm size obtained by fracturing sintered pellets. The samples were heated in the Knudsen-cell either following an arbitrary temperature programme, or under constant temperature rate. In order to obtain the best resolution of the release rate peaks, frequent MS measurements were performed. Therefore, only few windows could be opened in addition to that of ^4He, corresponding to species produced by matrix sublimation, and, for irradiated fuel, to volatile fission products. The temperature rate was chosen in order to obtain complete release of helium below 2100 K, so that the gas depleted sample could be further heated under high sublimation rate conditions until total vaporisation. We could thus ensure that no helium was retained in some internal pockets of the sample; consequently, the fractional release could be accurately normalised to the total initial helium content. The absolute value of this latter was in most cases deduced from reliable burn-up and/or radioactive decay calculations. In the case of thermally dissolved helium, the effusion cell calibration factor had to be used.

Table 1
Sample description

Samples	Exp. nr/ quality	Conditions	Weight (g)	Pu content (g)	He (mol/g) (calculated)	He (mol/g) (measured)	Error (mol/g)
Pre-melted UO_2 (fragments)	1/***	Sintered UO_2 heated above T_m in 2000 bar He	0.05	–	–	3.8×10^{-7}	1×10^{-7}
	2/***	Idem	0.05			3.7×10^{-7}	
Sintered PuO_2 (very fragile fragments)	3/**	PuO_2 sintered 25 years aged	0.300	0.264	2.62×10^{-6}	3.4×10^{-6}	0.6×10^{-6}
	4/*	PuO_2 sintered 25 years aged	0.270	0.238		2.6×10^{-6}	
	5/**	PuO_2 sintered 25 years aged	0.353	0.311		2.6×10^{-6}	
	6/**	PuO_2 sintered 25 years aged	0.301	0.264		1.9×10^{-6}	
$(^{238}PU_{0.1},UO_{0.9})O_2$ (fragments)	7/****	$U_{0.9}Pu_{0.1}O_2$ sintered co-precipitated 2 years aged	0.073	5.17×10^{-3}	4.66×10^{-6}	3.6×10^{-6}	0.6×10^{-6}
	8/****	$U_{0.9}Pu_{0.1}O_2$ sintered co-precipitated 2 years aged	0.032	2.54×10^{-3}		4.2×10^{-6}	
	9/****	$U_{0.9}Pu_{0.1}O_2$ sintered co-precipitated 2 years aged	0.039	3.26×10^{-3}		5.1×10^{-6}	
MOX (fragile fragments)	10/***	$U_{0.82}Pu_{0.18}O_2$ sintered blended powder 25 years aged	0.124	0.02	4.86×10^{-7}	3.0×10^{-7}	1×10^{-7}
Irradiated UO_2 (fragments)	11/**	Sintered UO_2 (RIM structure); b.u.: 100 GWd/t, T_{irr}: ~500 °C, cooling time: 10 years	0.018	1.1×10^{-4}	1.98×10^{-6}	2.4×10^{-6}	0.8×10^{-6}
Irradiated MOX (fragments)	12/**	$U_{0.93}Pu_{0.07}O_2$ sintered blended powder; b.u.: 18.7 GWd/t, T_{irr}: 500 °C, cooling time: 15 years	0.013	5.16×10^{-4}	1.58×10^{-6}	1.9×10^{-6}	0.6×10^{-6}
	13/**	$U_{0.96}Pu_{0.04}O_2$ sintered blended powder; b.u.: 42.6 GWd/t, T_{irr}: 700 °C, cooling time: 15 years	0.014	1×10^{-4}	3.44×10^{-6}	2.2×10^{-6}	
	14/**	$U_{0.96}Pu_{0.04}O_2$ sintered blended powder; b.u.: 44.4 GWd/t, T_{irr}: 500 °C, cooling time: 15 years	0.016	1.2×10^{-4}	3.56×10^{-6}	3.1×10^{-6}	
	15/**	$U_{0.93}Pu_{0.07}O_2$ sintered blended powder; b.u.: 23.0 GWd/t, T_{irr}: 500 °C, cooling time: 15 years	0.021	8.3×10^{-4}	1.55×10^{-6}	2.0×10^{-6}	

Quality of the test and consequent fitting precision: **** 300–400 points: 5% precision, *** 200–300 points: 5% precision, ** 100–200 points: 10% precision , * 50–100 points: 15% precision.

4. Method of helium release analysis

For the different types of samples examined, representative fractional release curves have been obtained as functions of time and annealing temperature.

Though their shape depends in part on the applied thermal annealing programme, substantial differences due to the ruling diffusion mechanisms could be realised. Their interpretation in term of a simple, single-energy activated diffusion processes resulted to be fully inadequate.

Table 2
Analysed spent-fuel samples: irradiation conditions and calculated helium formation (ORIGEN)

Type of fuel	Initial fissile atom enrichment (%)	Burn-up (GWd/t)	APEIT (days)	Neutron flux $(cm^2\ s)^{-1}$	He at EOL (mol/g)	He at EOS (mol/g)
MOX low b.u.	6.9 (^{239}Pu)	19	260	1.16×10^{14}	0.096×10^{-6}	1.58×10^{-6}
MOX medium b.u.	3.5 (^{239}Pu)	42.6	1264	1.59×10^{14}	1.39×10^{-6}	3.50×10^{-6}
UO_2	25.8 (^{235}U)	100	n.a.	n.a.	0.57×10^{-6}	1.98×10^{-6}

APEIT: average-power equivalent irradiation time; EOL: end of life; EOS: end of storage; n.a.: data not available for publication.

A more detailed approach had to be followed in the analysis, by maintaining, however, the interpretation perspective as wide as possible. In the examined experiments, the analysis is facilitated by the initial uniform distribution of helium in the samples. Due to its build-up or intake conditions, an important fraction of gas at the start of the annealing experiments was dynamically or thermally dissolved in the oxide lattice. We have, therefore, assumed the most general affordable hypothesis concerning the gas diffusion leading to the measured release. This provides two essentially different paths described by the following reaction rate equation system in the tree variables c (gas amount in solution), b (amount trapped), and g (amount released):

$$\begin{aligned}\frac{dc}{dt} &= -Kc - (H+S)c,\\ \frac{db}{dt} &= Kc - Ub,\\ \frac{dg}{dt} &= (H+S)c + Ub.\end{aligned} \tag{1}$$

The structure of these differential equations is self-explaining. If the total initial gas amount is expressed as the sum of $c_0 = c(0)$ and $b_0 = b(0)$, the fraction dissolved, $c(t)$, is decreasing due to trapping (at a rate K) or de-sorption (at a rate $H+S$). The gas trapped, $b(t)$, is subsequently allowed to be released at a different rate, $Ub(t)$. Furthermore, the de-sorption rate is written as the sum of two terms; the first one has a coefficient (H) that is related (and counteracted) by the trapping rate coefficient, i.e., $H = f(K)$, whilst the second one (S) represents a fully independent de-sorption mechanism.

Release can be, therefore, achieved trough the two paths: $c \to g$ and $c \to b \to g$, as shown in the sketch of Table 3.

A priori, none of the reaction rate constants of Eq. (1) is known. These can be, however, expressed as products of a distinct diffusion coefficient $D = D_0^j \exp(-E_j/RT)$ and a constant, A_j, depending on the boundary morphology of the diffusion domain. The index $j = 1,\ldots,4$ corresponds to the four rate mechanisms H, K, S and U. In the absence of detailed information on the ruling diffusion mechanisms and on the nature and distribution of the sinks, we are here not particularly interested in a formulation of these pre-exponential constants. We shall only mention that the two concurrent mechanisms K and H are by definition governed by the same diffusion coefficient. Furthermore, in a simple model where release is achieved by migration to the boundaries of grains disseminated with traps, we have:

Table 3
Scheme of the release mechanisms analysis

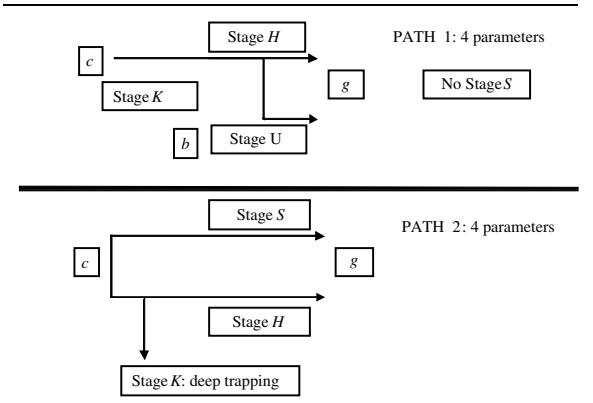

$$K = A_K D = k_{sc}^2 D_0 \exp(-E_j/RT), \tag{2}$$

where k_{sc} is the sink strength of the traps. If we now assume that the traps are affecting the long-range diffusion rate Hc in a domain of size $2a$ (a sintered grain in this case), the coefficient H has the expression [1]:

$$\begin{aligned}G &= -\frac{D}{Ka^2} + \frac{\coth a\sqrt{\frac{K}{D}}}{a\sqrt{\frac{K}{D}}},\\ H &= A_H D \equiv (k_{sc}^{gb})^2 D = \frac{3KG}{1-3G},\end{aligned} \tag{3}$$

for sufficiently large k_{sc} is: $H \to 3D\frac{k_{sc}}{a}$.

The rate coefficients K (trapping) and H (long-range diffusion) are governed by the same elementary gas migration process, and hence have a similar dependence on temperature; however, their magnitudes are defined by some parameters respectively defining the morphology of the traps and of the encompassing diffusion domain.

In ideal cases k_{sc} may assume simple expressions: e.g., for N spherical gas bubbles of radius r is $k_{sc}^{b} = (4\pi rN)^{1/2}$; for dislocations $k_{sc}^{d} = \rho^{1/2}$, where ρ is their density (i.e., their total length per unit volume). Thus, the ratio of trapping to long-range diffusion is inversely proportional to the ratio of two linear lengths representing the respective topological sizes of their domains of influence.

Now, if t' is the cumulative annealing time, and during the time interval $t = t' - t_0$ the temperature is not varied, equation system (1) has constant coefficients, and can be solved analytically. The following general integral is obtained:

$$\begin{aligned} c(t) &= c_0 e^{-(H+K+S)t}, \\ b(t) &= \frac{K e^{-Ut}[c_0(e^{-(H+K+S)t} - 1) + b_0(H+K+S-U)]}{H+K+S-U}, \\ g(t) &= e^{-Ut}\left[e^{Ut}(b_0 + c_0 + g_0) - \frac{c_0 K + b_0(H+K+S-U)}{H+K+S-U} - \frac{c_0 e^{(H+K+S-U)t}(H+S-U)}{H+K+S-U}\right], \\ H &= A_H e^{-\frac{E}{RT}}; \quad K = A_K e^{-\frac{E}{RT}}; \quad S = A_S e^{-\frac{E_S}{RT}}; \quad U = A_U e^{-\frac{E_U}{RT}}, \end{aligned} \tag{4}$$

where

$$c_0 = c(t_0); \quad b_0 = b(t_0); \quad g_0 = g(t_0).$$

Function $g(t)$, representing the fractional release, can thus be calculated with high accuracy for any programmed temperature $T = T(t')$ and used to fit the experimental curve $g_{exp}(T(t'))$. The only required conditions are the values of c_0, b_0 and g_0 at $t = 0$, i.e., at the beginning of the laboratory thermal annealing. In most of the examined samples was $c_0 \approx 1$ and $b_0 \approx 0$, $g_0 \approx 0$. Only in the reactor irradiated samples one could not exclude that part of the gas was precipitated during irradiation. However, the calculated concentrations reported in Table 2 indicate that in the low burn-up MOX most of the helium was produced during storage at ambient temperature, whilst in the medium burn-up MOX and the high burn-up UO_2 the amount produced in pile was of the same order of magnitude as that formed during storage. However, these fuels were irradiated at low in-pile temperatures so that the gas was likely kept in dynamical solution during irradiation. The assumption $c_0 \gg b_0$ and $g_0 \approx 0$ [1] was therefore plausible for all the examined samples.

[1] In the context of the rate equation approximation, the assumption of $g_0 = 0$ is legitimate as $g(t)$ is defined and referred to as the fraction of gas released during the laboratory annealing. Furthermore, it can be seen that the sensitivity of the fitting parameters of the normalised function $F = g(t)/(c_0 + b_0)$ on b_0 and c_0 is in our context not crucial. In practice, in the performed fitting procedures, an uncertainty of b_0 of the order of 20–30% results in a comparable uncertainty of the parameters A_j in Eq. (4) – i.e., of the height of the peaks of the different release stages – but has however a negligible effect on the resulting activation enthalpies.

It is obviously impossible to obtain from a numerical fitting the seven parameters of the general solution of Eq. (1). We have, therefore, considered only the two typical sub-cases mentioned above.

- In Path 1, helium is diffusing to free surfaces in the presence of concomitant trapping; both processes are controlled by the same elementary diffusion mechanism. In a following stage, the gas trapped diffuses to the free surface via a different diffusion mechanism.
- In Path 2, trapping is definitive and helium can only be released by matrix sublimation, however, unhindered long-range diffusion and release of atomic gas is allowed.

5. Results of the helium release analysis

5.1. Reactor irradiated UO_2

In the reactor irradiated samples – taken from the periphery of LWR fuel pellets – helium release was directly compared with that of xenon. In this type of samples, diffusion of xenon was examined in more detail in a previous work [1]; the atomic diffusion enthalpy of xenon was found to decreases with burn-up, from 103 kcal mol^{-1} in virgin fuel, down to 80 kcal mol at 100 GWd/t. The fuel samples examined here were irradiated at low temperature up to a high local burn-up (95–100 GWd/t) and, as expected, they exhibited at end-of-irradiation the typical RIM restructuring, consisting of formation of sub-grain cells of a tenth of micron size. The helium present in the fuel samples was likely distributed in lattice, in small intragranular bubbles and in pores, whereby the RIM restructuring has certainly produced a substantial gas precipitation into pores. On the other hand, helium initially present in the pressurised fuel rod may also have been in part absorbed or trapped in the fuel, so that the laboratory release analysis is facing a greater uncertainty than in the case of the other examined samples. Yet, as shown in Tables 1 and 2, the largest fraction of helium was created and dynamically dissolved in the lattice during post-irradiation storage by decay of actinides.

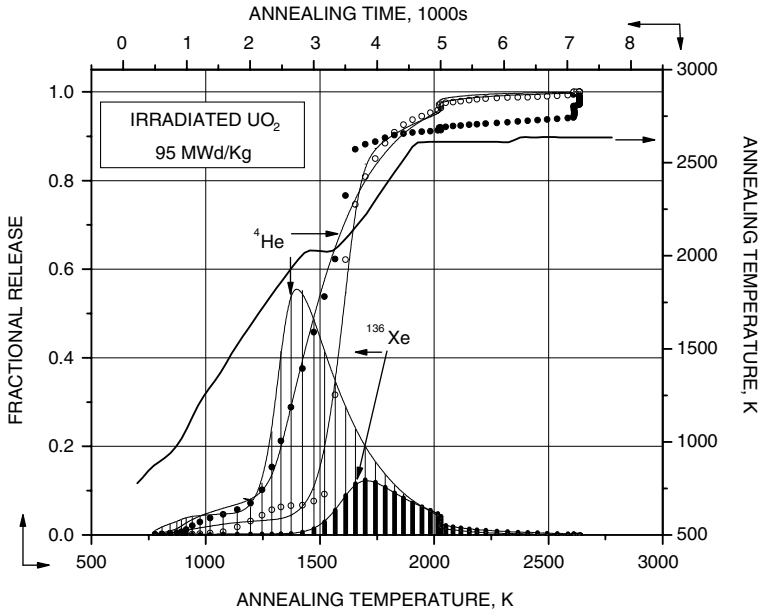

Fig. 2. Release of helium and xenon from a UO_2 fuel irradiated at low temperature up to 95 GWd/t. The symbols represent the experimental points and the full lines the theoretical fitting. The curves with drop lines represent the amount of gas trapped and subsequently released in Stage *U* as a function of the temperature programme that is plotted with the *y*-axis at the right-hand side.

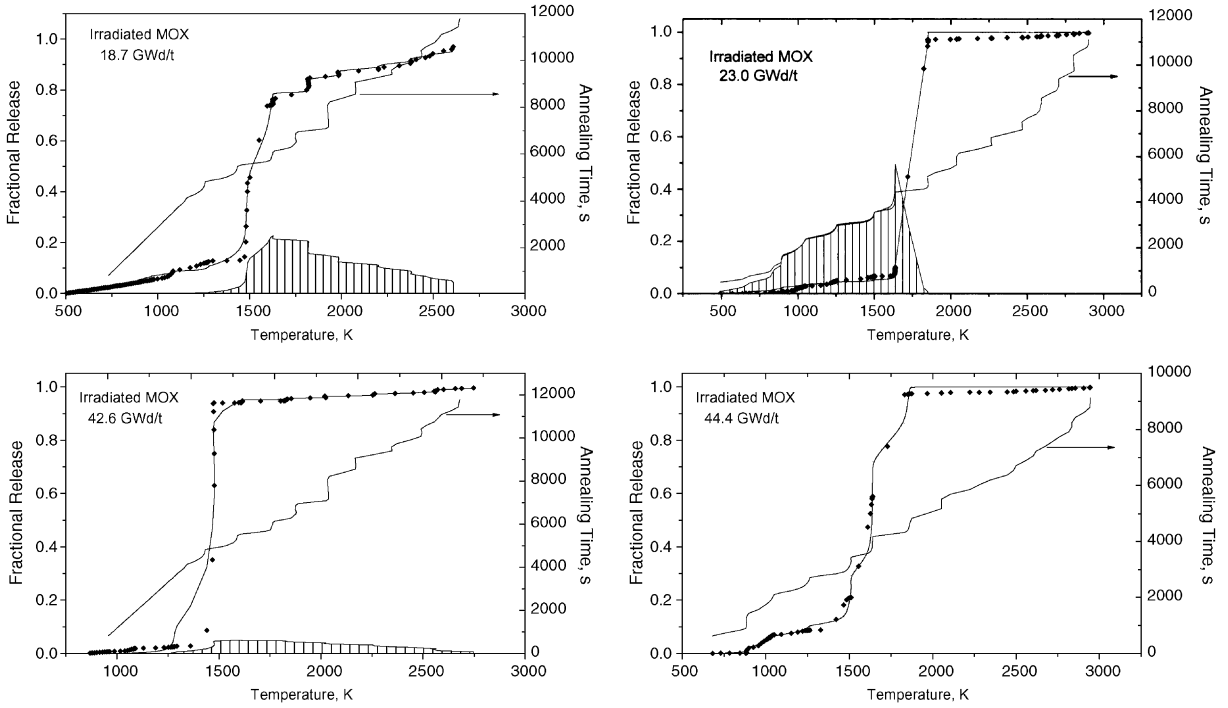

Fig. 3. Release of helium from four MOX fuels irradiated at different burn-ups at low temperature. The symbols represent the experimental points and the full lines the theoretical fitting. The curves with drop lines represent the amount of gas trapped and subsequently released in Stage *U* as a function of the temperature programme that is plotted with the *y*-axis at the right-hand side.

Table 4
Results of the gas diffusion analysis

Sample	Stage K: trapping on extended defects			Stage H: long-range atomic diffusion I			Stage S: long-range atomic diffusion II			Stage U: diffusion on extended defects		
	ΔE_K (kcal/mol)	A_K (1/s)	Fraction involved (%)	ΔE_H (kcal/mol)	A_H (1/s)	Fraction involved (%)	ΔE_S (kcal/mol)	A_S (1/s)	Fraction involved (%)	ΔE_U (kcal/mol)	A_U (1/s)	Fraction involved (%)
Reactor irradiated samples												
Xe in UO_2 100 GWd/t	80	4.2×10^{7}	10	80	2.7×10^{9}	90	–	–	–	18	2.1×10^{-3}	10
He in UO_2 100 GWd/t	70	1.4×10^{9}	56	69	2.2×10^{8}	44	–	–	–	Low	2.1×10^{-3}	56
He in MOX ~20 GWd/t	70	5.2×10^{6}	28	70	1.3×10^{7}	72	–	–	–	8.9	2.1×10^{-3}	28
He in MOX ~40 GWd/t	60	1.0×10^{5}	5	60	1.9×10^{6}	95	–	–	–	24	8×10^{-2}	5
Samples containing helium from α-decay												
He in $(U_{0.9},{}^{238}Pu_{0.1})O_2$ solid solution 2 years aged	46.5	5.9×10^{5}	41	46.5	4.1×10^{5}	59	–	–	–	19	4.5×10^{-1}	41
MOX 18%Pu mechanically blended 25 years aged	45.1	9.4×10^{5}	66	45.1	5.1×10^{5}	34	–	–	–	12	7.6×10^{-2}	66
He in PuO_2 25 years aged	40	6.2×10^{8}	81	40	–	19	–	–	–	1.8	5.6×10^{-3}	81
Samples containing thermally dissolved helium												
He-in-UO_2 single crystal 2000 bar He thermally dissolved at 3150 K	–	–	–	46.7	1.7×10^{2}	58	Low	6.9×10^{-6}	42	–	–	–

The release measurements were therefore mainly pertaining to this gas. As for helium formed during irradiation, different hypotheses were made from which a conservative error analysis was deduced (see Table 3).

It was found that helium release is dominated by atomic diffusion to the sub-grain boundaries, whilst only ~10% of the gas inventory was captured during thermal annealing by finely dispersed intragranular bubbles [2]. These samples were therefore suitable for comparing the atomic mobility of xenon and helium in a highly damaged lattice.

Fig. 2 shows the helium release measurements and that of ^{136}Xe, with the respective fitting curves. The release schemes 1 and 2 were applied, but only the first one was found to be suitable for an adequately precise fitting. The resulting diffusion enthalpy of xenon is 79 kcal mol^{-1}, in agreement with our previous results, and 69 kcal mol^{-1} for helium. According to the diffusion scheme compatible with the experiment, after reaching intermediate traps, the gas further migrates to free surfaces at a rate weakly dependent on temperature, the effective activation enthalpy being lower than 10 kcal mol^{-1}. In Fig. 2 both the fractional release and the calculated fraction of gas released after trapping are plotted versus annealing temperature. It can be seen that more than 80% of helium is reaching extended lattice defects – still unidentified – on which diffusion is faster than in the bulk. Only approximately 10% of the inventory is apparently trapped in deep sinks from which release occurs only by sample sublimation.

5.2. Reactor irradiated MOX (heterogeneous sintered fuel)

Various samples were taken from 15 years old LWR MOX rods irradiated between 18 and 44 GWd/t. At low burn-up the helium release curves are analogous to those of UO_2 (Fig. 3). During laboratory annealing, approximately 70% of helium migrates to the free surface with activation enthalpy of 70 kcal mol^{-1}, whilst 30% is trapped on extended defects and then migrated to free surface with very low activation enthalpy. From the pre-exponential factor of Stage K (Table 4) one can see that in MOX the trap spacing is approximately ten time larger than in high burn-up UO_2. At 44 GWd/t burn-up the release pathway does significantly change: 95% of the gas diffuses directly to the free surface with activation enthalpy of 60 kcal mol^{-1} and only 5% is passing through intermediate traps. Considering that the material was heterogeneous, and that the majority of measured helium was produced during the post-irradiation storage, one has to consider these data with caution. However, they appear to be consistent with those obtained in mixed oxides under different conditions.

5.3. α-helium in ^{238}Pu-doped UO_2

These samples were solid solutions of $(Pu_{0.1},U_{0.9})O_2$ where Pu was the highly alpha active ^{238}Pu isotope. The sample had been stored under ambient conditions during 2 years. The calculated amount of helium created is reported in Tables 1 and 2. The helium fractional release curves are plotted in Fig. 4.

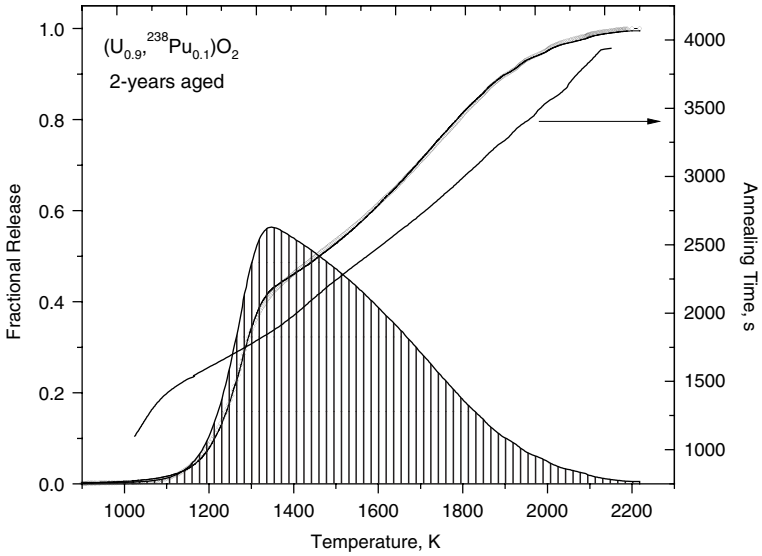

Fig. 4. Release of helium from a solid solution mixed oxide doped with ^{238}Pu. The experimental points are here completely covering the fitting curve.

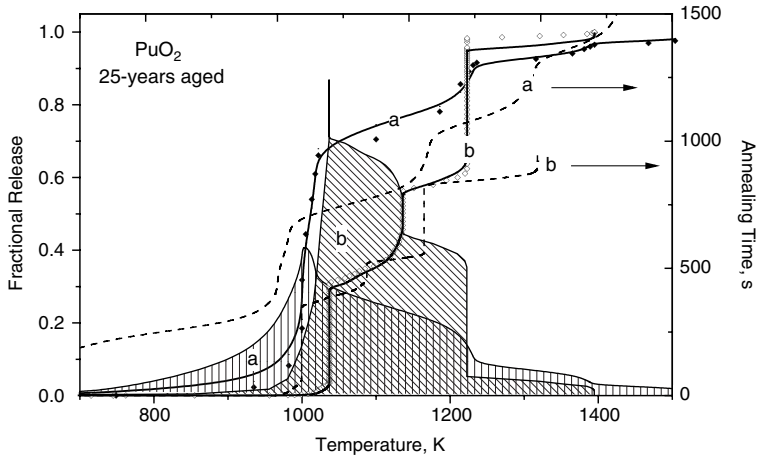

Fig. 5. Release of helium from sintered PuO_2 from two experiments with different temperature programmes. The symbols represent the experimental points and the full lines the theoretical fitting. The curves with drop lines represent the amount of gas trapped and subsequently released in Stage *U* as a function of the temperature programmes that are plotted with the *y*-axis at the right-hand side.

Also in this case, Path 1 had to be applied to obtain a satisfactory fitting. We obtained for atomic helium diffusion an enthalpy of 46.5 kcal mol^{-1}, with 60–70% of helium trapped and released via a low-energy activated mechanism.

5.4. α-helium in PuO_2

Helium release from nuclear-grade $^{239}PuO_2$ sintered pellets was measured after 25 years ageing and alpha-decay. The same release scheme was applied, obtaining, however, lower activation enthalpy (40 ± 2 kcal mol^{-1}) for helium atomic diffusion. In these samples the helium fraction trapped and subsequently released is larger than in $(U,Pu)O_2$, amounting up to 80–90% of the helium inventory (Fig. 5).

5.5. Helium thermally dissolved in UO_2

Helium was dissolved in these samples by infusion during laser heating pulses under 2000 bar helium and peak temperatures just above the melting point of UO_2. The sample, initially stoichiometric, was melted during a few seconds, and then rapidly cooled down at a rate of the order of magnitude of 10^5 K s^{-1}. During these pulses the O/U ratio was slightly displaced toward hypo-stoichiometry since congruent vaporisation of UO_2 is occurring at O/U = 1.98. Fragments of 50 mg weight of the melted pool were then extracted and used for helium release measurements. The amount of helium found in these specimens was of the order of 100 at. ppm. Based on the available experimental conditions, one cannot establish how far this concentration from the solubility limit of helium in UO_2 is. The helium release curve in these samples presents essentially different features (Fig. 6). Only Path 2 results to be adequate for fitting. This consists of two parallel diffusion processes without mutual interference. The first one, involving 60–80% of the helium inventory, has 46.7 ± 0.5 kcal mol^{-1} activation enthalpy, while the rest of the gas (40–20%) is released with activation enthalpy of magnitude below the significant level.

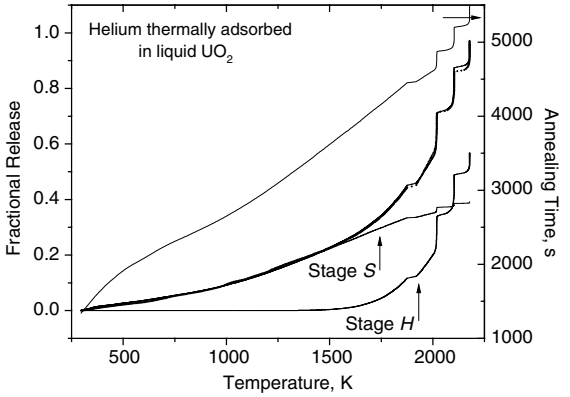

Fig. 6. Release of helium from UO_2 melted under 2000 bar helium. The symbols represent the experimental points and the full lines the theoretical fitting. The calculated contributions of Stage *H* and Stage *S* (Path 2) are also plotted.

5.6. Diffusion coefficient of atomic helium

Deduction of the pre-exponential factor D_0 of the helium diffusion coefficient is facing the problem of sufficiently defining the spatial boundary conditions of the process involved and the involved sink strengths. Factorisation of D_0 in the two coefficients A_H and A_K

respectively defined in Eqs. (2) and (3) is, however, possible if the grain boundary size is assumed as a representative dimension of the average distance to the extended defects on which the secondary stage S occurs. Fitting of the experimental curves with the additional *fifth* parameter D_0 requires a very accurate experimental dataset. In fact, only the release curves of the ^{238}Pu-doped mixed oxide samples were sufficiently smooth to enable a five parameter fitting to be significantly carried out. The results provide an expression of the helium atomic diffusion coefficient as follows:

$$D = (8 \pm 2) \times 10^{-7} \times \exp\left[(-46\,000 \pm 500)\ \mathrm{cal\,mol^{-1}}/RT\right]\ \mathrm{m^2\,s^{-1}}. \quad (5)$$

The figures refers to a solid solution $(Pu_{0.1},U_{0.9})O_2$ with stoichiometric composition.

6. Discussion

The results of the helium release analysis are collected in Table 4. One can see that the primary diffusion enthalpy of helium exhibits a marked variation as a function of the initial state of the sample. In irradiated UO_2 this enthalpy is high (69 kcal mol^{-1}), a value barely below that of xenon, whose state in reactor irradiated fuel is highly stabilised and mostly associated to Schottky trios. One can infer that the helium atoms are also trapped in this kind of vacancy clusters, which are present in the heavily damaged fuel lattice, and that jumps out of these stable configurations are not very effective. Probably a vacancy-assisted mechanism is necessary for helium diffusion, which is expected to be directly related to the damage annealing process. The smaller diffusion enthalpy with respect to that of xenon is likely due to the low saddle potential barrier for the helium atom. In fact, computer simulations of defective UO_2 lattice indicate that the energy barrier to helium migration in a U- or O-vacancy-assisted mechanism is of the order of magnitude of only a few tenth of eV [3].

The situation is very similar in the low burn-up irradiated MOX. Despite the heterogeneity of this mixed oxide, the analysis reveals that the atomic diffusion mechanisms are the same and the activation energy very close to that in UO_2. The only relevant difference is in the pre-exponential factor (lower value of A_K), which indicates a longer characteristic migration distance with respect to that in irradiated UO_2. This is understandable in a structure where the release pathway extend over large areas of almost intact sintered structure.

In the $(^{238}Pu_{0.1},U_{0.9})O_2$ solid solution and in PuO_2 we also found that the measured release could be very well described by Path 1. The respective activation enthalpy (46.5 and 40 kcal mol^{-1}) is, however, in both materials lower than in irradiated UO_2. In these two materials the deduced sink strengths of the traps are also different by one order of magnitude.

Helium release in non-irradiated heterogeneous, mechanically blended MOX shows an essentially different behaviour. Analysis of the release curves clearly indicates that Path 1 must be adopted. The atomic diffusion enthalpy (45.1 kcal mol^{-1}) is very near to that of the homogeneous mixed oxide. Only the pre-exponential factor A_H is by one order of magnitude smaller, indicating that the gas had to diffuse over a proportionally longer MSQ distance to reach the next free surface.

Helium injected in the lattice from α-decay comes also to rest in a similar highly stabilised form. Though one alpha-decay event creates a few hundred lattice displacements (against tens of thousand produced by fission fragments) the damage accumulated by the examined 'α-doped' materials is at first sight similar to that produced in reactor (transmission electron micrographs of high burn-up fuel and of 'α-doped' mixed oxides are shown in Figs. 7 and 8. However, the damage annealing processes are essentially different due to the presence in the irradiated fuel of high concentrations of fission products which tend to capture the available U-vacancies to form bubbles and low density precipitates. In fact, in 'α-doped' samples the measured diffusion enthalpy is nearer to that of thermally dissolved atoms.

The specimens used were sufficiently large to exhibit representative effects of the sintered structure in the release stages. Grain boundary or, more generally, extended defects do certainly define the role and extent of bulk atomic diffusion. It is remarkable that in all the irradiated samples long-range atomic diffusion (Stage H) involves a large percentage of the helium inventory. This indicated that the grain boundaries are sufficiently cov-

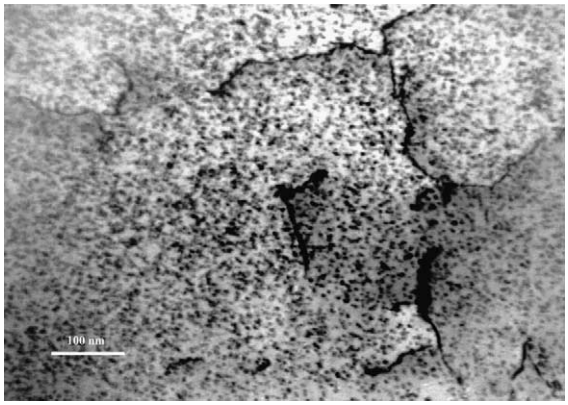

Fig. 7. Transmission electron micrograph of UO_2 irradiated in reactor to 95 GWd/t burn-up at a temperature of approximately 800 K.

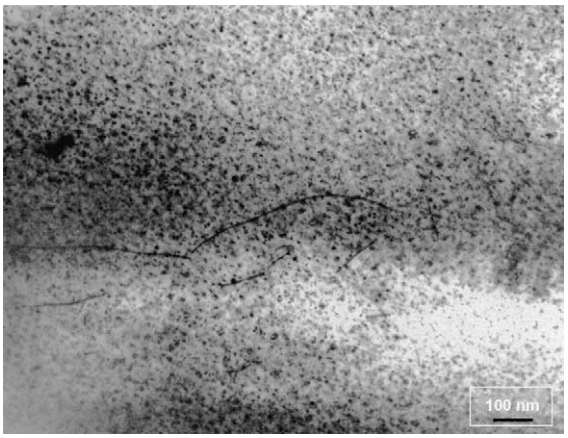

Fig. 8. Transmission electron micrograph of UO_2: 10% $^{238}PuO_2$ after 2 years aging under ambient conditions.

ered by a system of interconnected channels to let percolate the gas without any significant delay. A small percentage is effectively trapped and has to work out his way to a free surface by migrating with an uncertain, low diffusion enthalpy (Stage *U*). Yet, it should be noted that, numerically, such low enthalpies imply an almost linear dependence of the release rate on temperature. The situation is reversed in alpha-doped samples: most of the gas is first trapped on extended defects and from there is released through a similar Stage *U*. It is remarkable that the characteristic rate of this stage differs in all the examined samples, and is comparatively low in mechanically blended oxide, where the release pathway has to cross large, structurally intact zones.

The results of release of helium thermally dissolved in UO_2 at 3150 K can be reasonably interpreted: approximately 60% of the gas is directly released via atomic diffusion (Stage *H*) with a relatively low activation enthalpy (46.7 kcal mol^{-1}) and a small pre-exponential factor, indicating a long migrated distance. This should be expected in samples that consist of crystals of a few hundreds of micrometers sizes. The second stage (*S*) – with insignificant activation enthalpy and involving 40% of the gas inventory – is not correlated with the former stage and must be due to gas adsorbed or segregated on extended defects during high temperature restructuring. The concentration of helium found in the samples reported in Tables 1 and 2 might be much lower than the saturation value. As for the effective infusion conditions of the examined samples, one should note that at 3150 K the free energy of helium increases of 47 kcal mol^{-1} if the pressure increases from 1 to 2000 bar.

This value is compatible with the measured activation enthalpy of Stage *H*, where gas dissolved thermodynamically in the lattice is involved. In this respect, the experimental observations are also in agreement with LMTO-ASA model calculations [4] of the solution energies of helium in octahedral sites (30 kcal mol^{-1}) and in oxygen vacancies (41 kcal mol^{-1}) in the case of hypo-stoichiometric UO_2. [2] In the stoichiometric oxide, the He solution energy in O-vacancy is obviously higher since the formation energy of an oxygen vacancy, deduced from neutron scattering data [5], is 3.67 eV. However, at high temperatures and, in particular, above the λ-transition at 2600 K – an order-disorder transition in the oxygen sub-lattice – the O-vacancy concentration increases up to the order of magnitude of 0.1 [6]. Therefore, the state of helium thermally dissolved in UO_2 and measured in the reported experiments likely corresponds to a stabilised configuration where the gas occupies an oxygen vacancy. A more decisive interpretation of these data will be obtained from a solubility study of helium in UO_2 at high temperatures. These measurements are in progress in our laboratory.

Finally, a few words are in order here on the deduced atomic coefficient of helium expressed by Eq. (5). From the data reported in Table 3 one can conjecture that the elementary diffusion mechanism pertains to helium in a O-vacancy, a configuration which seems to be predominant when the gas is created by α-decay, but which is also found under thermal infusion conditions. Within the experimental uncertainty, the activation enthalpy of 45.1 kcal mol^{-1} is in agreement with old measurements [7,8]. Other data published in the same years [9–11] show, however, a great dispersion, with estimated diffusion enthalpies ranging from 17 to 86 kcal mol^{-1}. The discrepancy between the various results depends in part on the quality of the measurements, but mainly on the type of analysis applied, which in the previous works was basically developed from inadequate diffusion models, whereby changes in mechanisms were only realised on the resulting Arrhenius plots: a too imprecise procedure for identifying overlapping operating mechanisms. The diffusion coefficient of Eq. (5) at temperatures between 1000 and 1500 K is up to four orders of magnitudes higher than that obtained in early works [9,10]. Actually, the evaluation of D_0 is always based on more or less founded assumptions, since in the integrals of the transport equation the quantity *D* is always multiplied by the square of a characteristic length, whose empirical meaning is not straightforward. It is however worthwhile noting that the magnitude of *D* at 1500 K in the above mentioned works is 1.5×10^{-17} m^2 s^{-1}. Now, no matter how the analysis of the release data is configured, the strong release onset at 1400 K, occurring in

[2] One should mention that previous calculations reported in Ref. [3] predict a small, negative energy of solution for helium in octahedral sites in stoichiometric and hypo-stoichiometric UO_2. This is evidently in disagreement with the experimental results.

all our experiments in a few tens of minutes, can hardly be explained if such a low atomic mobility is assumed.

7. Conclusions

- Helium diffusion in uranium, uranium/plutonium and plutonium dioxide was investigated from release measurements carried out in a Knudsen-cell provided with an on-line mass spectrometer. The samples were reactor irradiated fuels or fragments of sintered pellets doped with α-emitters, and sufficiently aged to accumulate a concentration of helium of the order of a few 100 ppm. Two samples were submitted to helium infusion at high temperature and high pressure.
- Analysis of the results indicates that release of helium cannot be described as a single-energy activated process. Atomic diffusion is mainly controlling short-range migration to still unidentified traps from which the gas subsequently migrates and escapes with a very low activation enthalpy, effectively at a rate proportional to temperature. The nature and sink strength of the traps essentially depends on the level of damage of the lattice. Also the diffusion enthalpy is markedly affected by this damage: it increases from 45 kcal mol^{-1} in nominally intact or moderately damaged lattice to 70 kcal mol^{-1} in fuel irradiated to 95 Gwd/t burn-up.
- Analysis of the reported experiments shows that helium mobility in these oxides is much higher (up to four orders of magnitude) than as previously published in the literature.
- Finally, the extremely low activation enthalpy associated to the secondary release stage (probably migration on dislocation networks and grain boundaries) can be related to the observed dramatic embrittlement of sintered uranium and plutonium oxides supersaturated with helium.

Acknowledgements

The authors are greatly indebted to the ITU thermodynamic laboratory staff, in particular to F. Capone and J.Y. Colle for the dedicated collaboration in the experiments reported in this paper. A special thank is due to T. Wiss for the characterisation of the samples and for providing the TEM micrographs shown in this paper.

References

[1] C. Ronchi, J. Sakellaridis, C. Syros, Sci. Eng. 95 (1987) 282.
[2] F. Capone, J.P. Hiernaut, M. Martellenghi, C. Ronchi, Nucl. Sci. Eng. 124 (1996) 436.
[3] R.W. Grimes, R.H. Miller, C.R.A. Catlow, J. Nucl. Mater. 172 (1990) 123.
[4] J.P. Crocombette, J. Nucl. Mater. 305 (2002) 29.
[5] M.T. Hutchings, J. Chem. Soc. Faraday Trans. II 83 (1987) 1083.
[6] C. Ronchi, G.J. Hyland, J. Alloys Compd. 213&214 (1994) 159.
[7] J. Belle, Properties of UO_2, in: Proc. 2nd United Nations International Conference on Peaceful Uses of Atomic Energy, Geneva, 1958, vol. 6, p. 585.
[8] W.A. Stark, USA Report SC-DC-69, Sandia Laboratories, Albuquerque, NM, 1969.
[9] P. Sung, PhD thesis, University of Washington, Microfilm 68-9339, University Microfilms, Ann Arbor, MI, 1967.
[10] F. Rufeh, D.R. Olander, T.H. Pigford, Nucl. Sci. Eng. 23 (1965) 335.
[11] P. Angelini, R.E. McHenry, J.L. Scott, W.S. Ernst, USA Report ORNL-4507, Oak Ridge National Laboratory, TN.